Quantum Electronics **50** (4) 366–374 (2020)

https://doi.org/10.1070/QEL17287

Interference effects in the formation of the light bullet spectrum under axicon focusing

E.D. Zaloznaya, V.O. Kompanets, S.V. Chekalin, A.E. Dormidonov, V.P. Kandidov

Abstract. **Specific features of the anti-Stokes band of the light bullet supercontinuum spectrum under filamentation of 1900-nm femtosecond pulses, focused by an axicon in fused silica and calcium fluoride, have been experimentally, numerically, and analytically investigated. It is found that the formation of two or more light bullets in a filament leads to modulation of spectral components' intensity. The oscillation period of spectral components, defined as the wavelength interval between adjacent intensity minima, decreases with decreasing their wavelength. On a logarithmic scale, the relative change in the oscillation period in the spectrum is proportional to the spectral component wavelength and is independent of the pulse energy and the position of the light bullet formation region in the filament. It is established that the modulation in the spectrum is due to the interference of the broadband supercontinuum emitted by light bullets, and its period decreases with increasing interval between them.**

Keywords: *femtosecond filamentation, light bullet, axicon, Bessel–Gaussian beam, supercontinuum, interference model.*

1. Introduction

When studying the filamentation phenomenon, particular attention is paid to the analysis of femtosecond radiation in a Gaussian beam focused by an axicon. This focusing leads to the formation of an extended localisation domain of radiation in the central lobe of Bessel–Gaussian intensity distribution [1]. A rise in the femtosecond radiation intensity in the case of Kerr self-focusing causes generation of plasma channels. The interval on which a chain of plasma channels is formed for a Bessel–Gaussian beam is much longer than for a collimated Gaussian beam under filamentation in fused silica [2, 3] and in air [4]. The change in the wavefront curvature for a Gaussian beam incident on an axicon makes it possible to control the length of the chain of plasma channels under filamentation [5].

Femtosecond filamentation is accompanied by generation of a broadband supercontinuum, which is due to the pulse self-phase modulation under conditions of Kerr self-focusing and defocusing in induced laser plasma [6–8]. Along with this, the concept of four-wave mixing [9] is applied to interpret the experimental results on spectral broadening, in particular, under filamentation of a 527-nm pulse focused by an axicon in water. Under filamentation of mid-IR radiation, with wavelengths lying in the anomalous dispersion region of group velocity in fused silica and fluorides, one can expect formation of light bullets (LBs) with high localisation of the light field due to the radiation compression in space and time [10]. An LB is a robust formation in a nonlinear dispersive medium; its path length is about 500 μm in beams focused by either an axicon or a lens [11]. When an LB is formed, an isolated anti-Stokes wing arises in the visible range of the supercontinuum spectrum; this wing is blue-shifted, and its shift increases and width decreases with an increase in the working pulse wavelength. At a pulse wavelength of 2200 nm, the wavelength of the isolated-wing maximum in the LB spectrum in fused silica does not exceed 500 nm [12–15]. The anti-Stokes wing maximum shifts from 550 to 400 nm in BaF_2 and to 330 nm in CaF_2 with an increase in the pulse wavelength from 3000 to 3800 nm [16] and from 800 to 250 nm in LiF with an increase in the pulse wavelength from 1460 to 3300 nm [17].

Due to the angular divergence of spectral components, the supercontinuum emission in the far-field zone forms a cone in the form of a continuous system of rainbow rings, whose radius monotonically increases with decreasing radiation wavelength in the supercontinuum spectrum [7]. When the pulse in filament is refocused, the radiation cone decomposes into a set of discrete rings [18]. With an increase in power, the pattern of discrete conical emission rings disappears in a collimated Gaussian beam because of the occurrence of multiple filamentation but remains stable against decomposition into many filaments in a Bessel–Gaussian beam [19].

The interference model [20] based on representing broadband supercontinuum radiation in the form of a coherent moving source, located at the pulse trailing edge (where the pulse intensity sharply drops due to defocusing in the induced laser plasma and the self-steepening effect), describes the properties of the formation of a conical emission frequency-angular spectrum. The interference model reproduces the conical emission angle-discrete spectrum from a sequence of supercontinuum sources, which arise in the filament under the refocusing caused by repeated compression of radiation in space, and during the LB chain formation, which is due to the multiple compression of radiation in time under anomalous group velocity dispersion conditions [16, 18, 21, 22]. The interference model was used to derive the dispersion equation for the shift of the anti-Stokes band maximum in the LB spectrum as a function of the working radiation wavelength [23].

E.D. Zaloznaya, V.P. Kandidov Faculty of Physics and International Laser Center, Lomonosov Moscow State University, Vorob'evy gory, 119991 Moscow, Russia; Institute for Spectroscopy, Russian Academy of Sciences, ul. Fizicheskaya 5, Troitsk, 108840 Moscow, Russia; e-mail: ed.zaloznaya@physics.msu.ru;
V.O. Kompanets, S.V. Chekalin, A.E. Dormidonov Institute for Spectroscopy, Russian Academy of Sciences, ul. Fizicheskaya 5, Troitsk, 108840 Moscow, Russia

Received 18 February 2020
Kvantovaya Elektronika **50** (4) 366–374 (2020)
Translated by Yu.P. Sin'kov

The validity of this equation is confirmed by all known results of experimental studies of the short-wavelength LB spectrum in the case of filamentation in SiO_2, BaF_2, CaF_2, LiF, and H_2O, under anomalous group velocity dispersion conditions for radiation with wavelengths varying in the range of 1400–4000 nm. Modulation in the supercontinuum spectrum on the filament axis was recorded in [8], when a 100-fs pulse at a wavelength of 800 nm was refocused in YAG during filamentation upon normal group velocity dispersion conditions.

In this paper, we report the results of studying the specific features of the supercontinuum anti-Stokes band spectrum during the formation (under conditions of anomalous group velocity dispersion) of an LB sequence in a filament obtained by focusing (with the aid of an axicon) a mid-IR beam into fused silica and calcium fluoride samples. The application of axicon focusing of femtosecond radiation provided a stable sequence of LBs and made it possible to record reliably their spectrum. Some new features of the formation of the mid-IR LB supercontinuum spectrum were revealed. The experimentally observed modulation of the spectrum during the formation of an LB sequence is confirmed by the results of numerical simulation and analytical study within the interference model. The change in the modulation period is found to depend on the spectral component wavelength.

2. Experimental

An experimental study of the anti-Stokes wing in the spectrum of LBs formed by axicon focusing of high-power femtosecond mid-IR laser radiation was performed on a unique research facility 'Multipurpose Femtosecond Laser-Diagnostic Spectrometric Complex' at the Institute of Spectroscopy of the Russian Academy of Sciences, which includes a tunable parametric amplifier (TOPAS) combined with a regenerative amplifier (Spitfire Pro). A schematic of the experimental setup is shown in Fig. 1.

The study was performed using a pulsed beam with the following parameters: pulse width (FWHM) ~90 fs, repetition rate 1 kHz, beam diameter (FWHM) ~2 mm, and wavelength $\lambda_0 = 1900$ nm, which correspond to the region of anomalous group velocity dispersion in fused silica and calcium fluoride. Radiation with a close-to-Gaussian transverse intensity profile was focused by a fused silica axicon with a base angle $\alpha = 5°$ into wedge-shaped samples of fused silica or calcium fluoride. Samples were mounted on a translation stage, which made it possible to move them perpendicular to the radiation propagation direction, thus changing the length of nonlinear optical interaction between radiation and dielectric, with radiation parameters being the same.

In the case of an axicon-focused Gaussian beam, there is a region where a Bessel–Gaussian intensity distribution is formed in the cross-sectional plane; it has a form of an intense central peak surrounded by weaker rings [1]. The axicon focal length Z_{bess}, at which the intensity in the central lobe of Bessel–Gaussian beam reaches maximum, depends on the axicon base angle and the incident-beam radius. For an axicon with an angle $\alpha = 5°$ and a beam radius $a_0 = 1.2$ mm (at an intensity level of e^{-1}), the focal length is $Z_{bess} = 22$ mm. When carrying out a series of experiments, the length b between the axicon tip and wedge flat face was varied from 6 to 28 mm, which made it possible to investigate the spectrum of an LB formed in the beam both before and behind the axicon focus. Thus, a beam with a Bessel–Gaussian structure formed in air was incident on the sample input face.

The anti-Stokes wing spectra were recorded using a fibre spectrometer (SL-40 Solar TII) in the wavelength range of 200–1100 nm. The supercontinuum radiation at the spectrometer input window was collected by a lens with a focal length $F = 8$ mm. The IR spectral region was cut off by an SZS-25 filter. Spectra of a series of pulses were recorded in the single-filamentation regime, which was implemented by varying the pulse energy from 30 to 110 μJ (measurements were performed with a Thorlabs S401C sensor). The luminescence of plasma channels (characterising the position and extension of regions of high energy localisation and, therefore, LB formation and supercontinuum generation) was recorded through the sample side face by a Nikon D800 camera with an exposure of about 20 s. The spectra recorded in fused silica at different exposure times did not change, which indicated the absence of accumulated dislocations in the sample during the measurements. In the experiments with calcium fluoride, where the spectrum changed in the multipulse detection mode, the sample was moved in the cross-sectional plane during the exposition.

Figure 2 shows a photograph of the plasma channels formed during the generation of a sequence of two LBs in the filament by a pulse with energy $W = 55$ μJ in a fused silica sample, located at a distance $b = 8$ mm from the axicon tip.

We recorded spectra in an aperture with an angular size $2\theta_0$ of about 0.1 rad for the detection scheme in use. An example of measured anti-Stokes wing spectra is shown in Fig. 3 for a fused silica wedge located at a distance of $b = 6$ mm from the axicon tip. In the case under consideration, the radiation path length in the wedge is $d = 8$ mm. At a pulse energy $W = 50$ μJ, only one LB was formed on the entire interaction length between the radiation and medium, which was detected from the presence of a single region of plasma recombination luminescence in the sample. The spectrum of

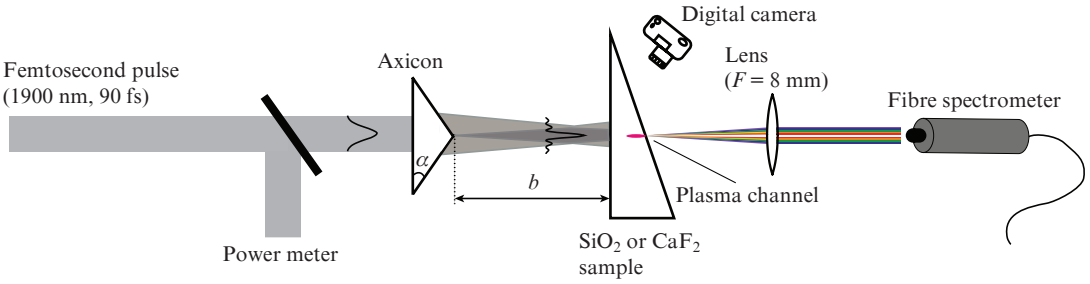

Figure 1. Schematic of the experimental setup.

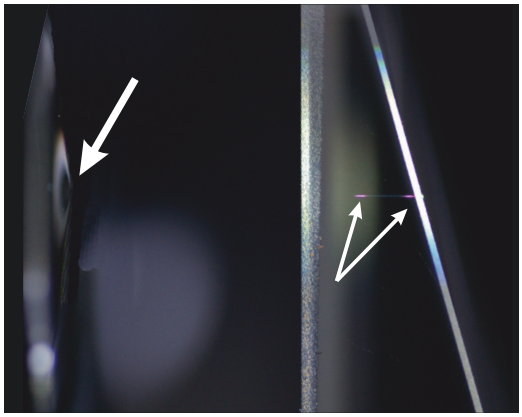

Figure 2. Plasma channels accompanying the formation of a sequence of two LBs in a wedge-shaped fused silica sample. Radiation propagates from left to right. The axicon tip and plasma channels are indicated by white arrows.

one LB gradually changes in the range of 450–650 nm (Fig. 3a). An insignificant rise in the initial radiation energy to $W = 51$ μJ resulted in the following: the power in the central lobe of the Bessel–Gaussian beam incident on a fused silica sample became sufficient to form another LB on the same nonlinear optical interaction length after the first one. In this case two plasma channels, spaced at a distance $L \approx 2.2$ mm along the filament, were observed through the sample side face (a pattern similar to that presented in Fig. 2). The components' intensity in the spectrum of two LBs becomes oscillating with a change in the wavelength (Fig. 3b).

After increasing the distance b between the wedge and the axicon up to 24–28 mm, measurements showed that one LB is formed in a fused silica sample and that oscillations are absent in the spectrum at the interaction length $d = 3.8$ mm, as well as in the case of a sample located before the axicon focus (see Fig. 3a). With an increase in the pulse path length in the sample and, as a consequence, rise in the nonlinear optical interaction length to $d = 8.5$ mm by moving the wedge perpendicular to the radiation propagation direction, a sequence of two LBs was formed (detected by the presence of two plasma channels). Its formation was accompanied by the occurrence of modulation in the spectrum of anti-Stokes wing, especially contrast in the range of 490–630 nm (Fig. 4a). Modulation was also observed during the formation of a sequence of several LBs in calcium fluoride. An example of the spectrum of several LBs in the CaF_2 sample located behind the axicon focus is shown in Fig. 4b.

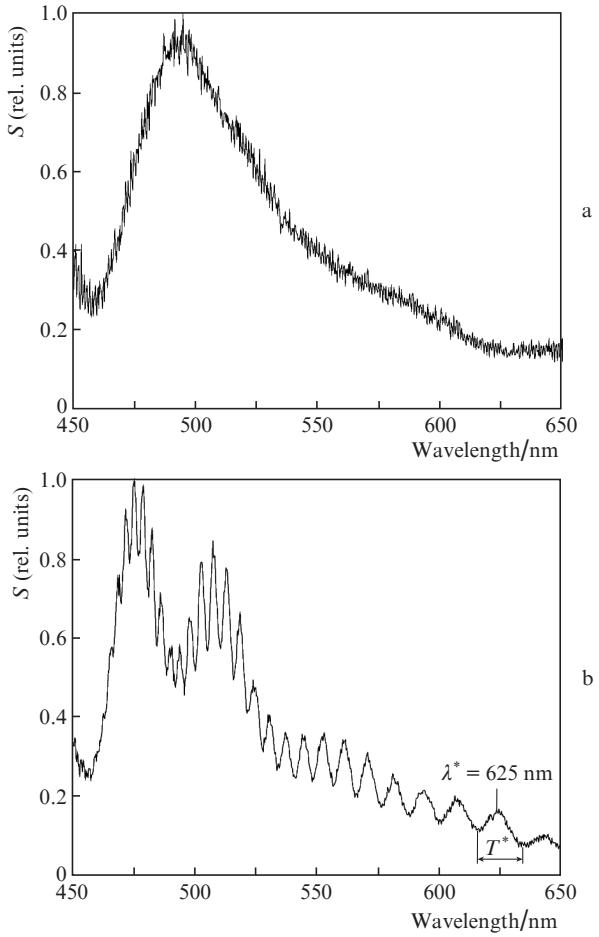

Figure 3. Experimental spectra of anti-Stokes wing in fused silica in the cases of (a) one LB at a pulse energy $W = 50$ μJ and (b) two LBs at $W = 51$ μJ. The distance from the axicon tip to the sample is $b = 6$ mm, and the sample length $d = 8$ mm.

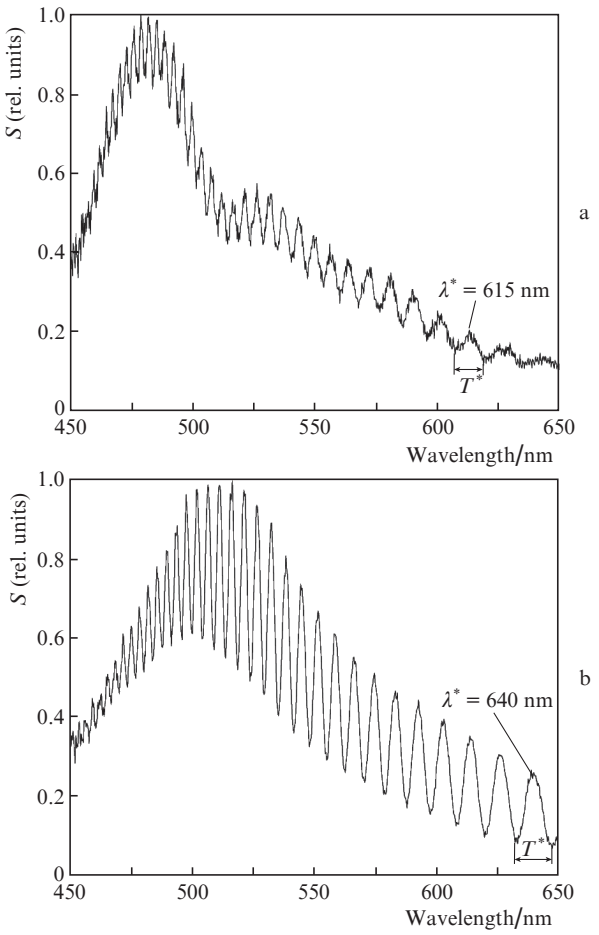

Figure 4. Experimental spectra in the cases of (a) two LBs in SiO_2 at $b = 28$ mm and $W = 42$ μJ and (b) several LBs in CaF_2 at $b = 24$ mm and $W = 69$ μJ.

Thus, independent of the sample position relative to the axicon focus, the spectral component intensity becomes modulated when several LBs arise. The focusing using an axicon, in contrast to the lens focusing, provides a stable sequence of LBs with deeply modulated spectral components' intensity.

An analysis of the experimental results obtained for different positions of the sample input face in the region of the Bessel–Gaussian beam formation behind the axicon shows that the oscillation period T, which is defined as the interval between the wavelengths of adjacent minima of components' intensity in the spectrum of two LBs, decreases with a decrease in the component wavelength λ. On a logarithmic scale, the dependence of the relative oscillation period of the intensity of spectral components, $\log(T/T^*)$, on their wavelength $\log(\lambda/\lambda^*)$ is presented in Fig. 5. The scale of T^* is taken to be the interval between neighbouring minima in the spectrum of the anti-Stokes wing at the wavelength λ^* chosen in its long-wavelength region (600–650 nm) (Figs 3b and 4).

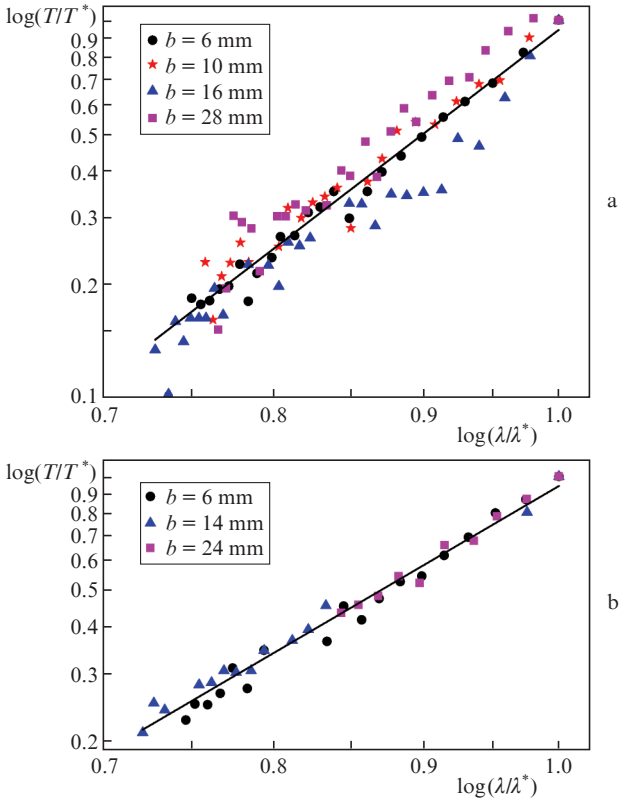

Figure 5. Relative change in the oscillation period T/T^* of the intensity of spectral components as a function of their wavelength λ/λ^* on a logarithmic scale, according to the results of measurements at different distances b between the axicon and the input face of (a) fused silica and (b) calcium fluoride samples. The solid line is an approximation of experimental results.

It can be seen that the relative change in the oscillation period T/T^* of spectral components on their wavelength λ/λ^* for LBs in CaF_2 (Fig. 5b) and SiO_2 (Fig. 5a), plotted on a logarithmic scale, obeys a linear dependence. The slope of the logarithmic dependence of the oscillation period on the wavelength is independent of the pulse energy and distance b between the axicon and sample.

3. Numerical simulation

The LB spectrum was numerically analysed using the slowly varying wave approximation, which makes it possible to consider the propagation and transformation of wave packets with a duration close to one oscillation period of the light field [24]. The analysis within this approximation took into account the diffraction and dispersion of the wave packet, generation of laser plasma, change in the refractive index due to the plasma and Kerr nonlinearities, and the radiation attenuation. The radiation at the axicon output was described by a Gaussian wave packet with a spatial phase modulation $\varphi(r)$:

$$A(r,t,z=0) = A_0 \exp\left[-\frac{r^2}{2a_0^2} - \frac{t^2}{2\tau_0^2} + i\varphi(r)\right], \quad (1)$$

where a_0 and $2\tau_0$ are, respectively, the beam radius and width of the Gaussian wave packet at an intensity level of e^{-1} and A_0 is the amplitude of the light field envelope. The axicon-formed spatial phase modulation is described by the expression

$$\varphi(r) = kr(n_{ax} - 1)\alpha, \quad (2)$$

where k is the wave number and n_{ax} is the refractive index of the axicon material. Expressions (1) and (2) do not take into account the nonlinear phase shift of the wave packet propagating in the axicon, because, according to the estimates within the specified-field approximation, the maximum of this phase shift is two orders of magnitude smaller than that in the samples prior to the LB formation.

The wave packet parameters from (1), used in numerical simulation, were chosen in correspondence with the experimental data: centre wavelength λ_0 = 1900 nm, width $2\tau_0$ = 108 fs, and radius a_0 = 1.2 mm. The simulation was performed for a wave packet propagating in air at a distance of b in the absence of nonlinearity and then for its nonlinear optical interaction in fused silica and calcium fluoride; i.e., the simulation completely imitated the experimental conditions.

As a result of the numerical simulation for the anti-Stokes supercontinuum wing, we determined the frequency-angular spectrum $S(\lambda,\theta)$ (θ is the angle of spectral component divergence), as well as the electron concentration $N_e(z)$ on the axis and the spatial and temporal intensity distribution $I(r,t)$ in the LB for a number of characteristic distances in fused silica and calcium fluoride samples and different conditions of laboratory experiment.

Figure 6 shows as an example continuous-tone patterns of the spectral intensity frequency-angular distribution $S(\lambda,\theta)$ of the anti-Stokes wing after the formation of one (Fig. 6a) and two (Fig. 6b) LBs in a fused silica sample located at a distance b = 6 mm from the axicon tip (energy W = 50 μJ).

It can be seen that one LB is formed on the interaction length d = 5.5 mm; the length path of this LB, determined by the plasma channel length, is about 300 μm [at a level of e^{-1} of concentration $N_e(z)$] (Fig. 7). The anti-Stokes wing spectrum $S(\lambda,\theta)$ in the case of one LB has a wide maximum at a wavelength of 550 nm and does not exhibit any periodic oscillations of the spectral component intensity (Fig. 6a). An increase in the interaction length d to 6.5 mm leads to the formation of a second LB (in a beam of the same power) after the first LB at a distance of L = 1.3 mm; this is evidenced by the occurrence of another plasma channel (see Fig. 7). The for-

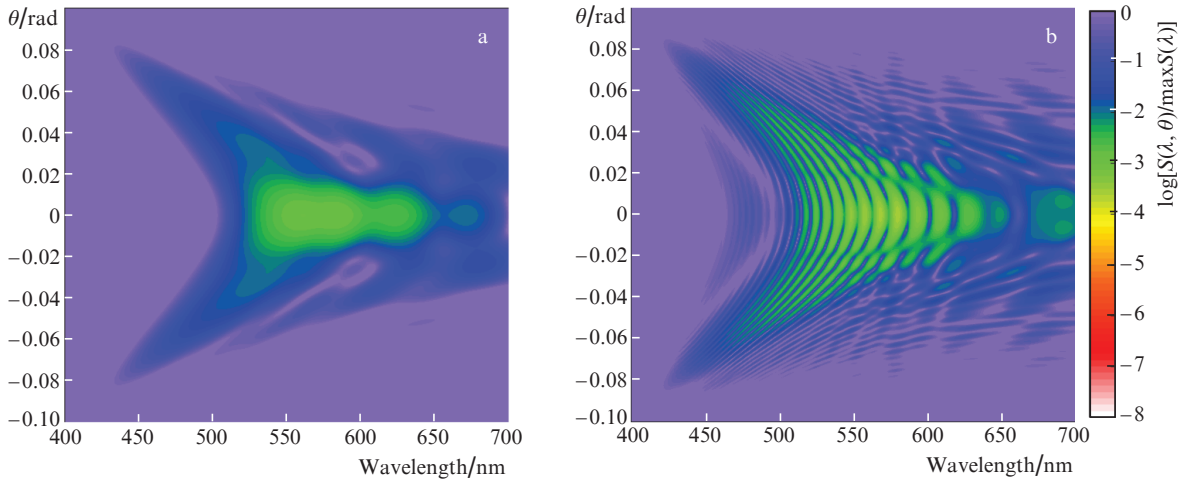

Figure 6. (Colour online) Numerically calculated anti-Stokes wing of the frequency-angular spectrum $S(\lambda,\theta)$ of a Gaussian wave packet with energy $W = 50$ μJ, focused by an axicon into a fused silica sample, during the formation of (a) one LB on the interaction length $d = 5.5$ mm and (b) two LBs on $d = 6.5$ mm. The distance between the sample and axicon tip is $b = 6$ mm.

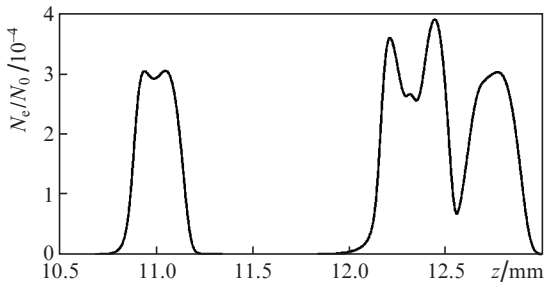

Figure 7. Free-electron concentration $N_e(z)$ on the axis in a fused silica sample, located at a distance $b = 6$ mm from the axicon tip. The radiation energy is $W = 50$ μJ, $N_0 = 0.21 \times 10^{21}$ cm^{-3} (z is the distance passed by radiation from the axicon tip).

mation of the second LB gives rise to many sharp minima in the frequency-angular spectrum $S(\lambda,\theta)$, which are due to the interference of the supercontinuum radiation from two coherent sources (LBs) (see Fig. 6b).

To compare the results of numerical simulation with the experimental data, we determined the total spectrum $S(\lambda)$ in the angular aperture $2\theta_0$ by integrating the spectral components' amplitude over angle θ within ±0.1 rad. The numerically calculated spectra $S(\lambda)$ of the anti-Stokes wing during the formation of one and two LBs in a wave packet in a fused silica wedge located at a distance $b = 6$ mm from the axicon (Fig. 8) coincide qualitatively with the experimental ones (Fig. 3).

The spatial and temporal intensity distribution $I(r,t)$ and its temporal profile on the axis $I(r=0,t)$ in the wave packet at a maximum intensity in the first and second LBs are presented in Fig. 9.

For the parameters under consideration, the peak power in the central lobe of the Bessel–Gaussian distribution exceeds the threshold power of the LB formation [25], and LBs arise specifically in the central maximum (Fig. 9a). In a Bessel–Gaussian beam, as well as in a Gaussian beam, the radiation compression in space and time due to the self-focusing and self-phase modulation under conditions of anomalous group velocity dispersion leads to an increase in the peak intensity and formation of an extremely squeezed high-intensity LB (Fig. 9a). As well as in the case of a Gaussian beam,

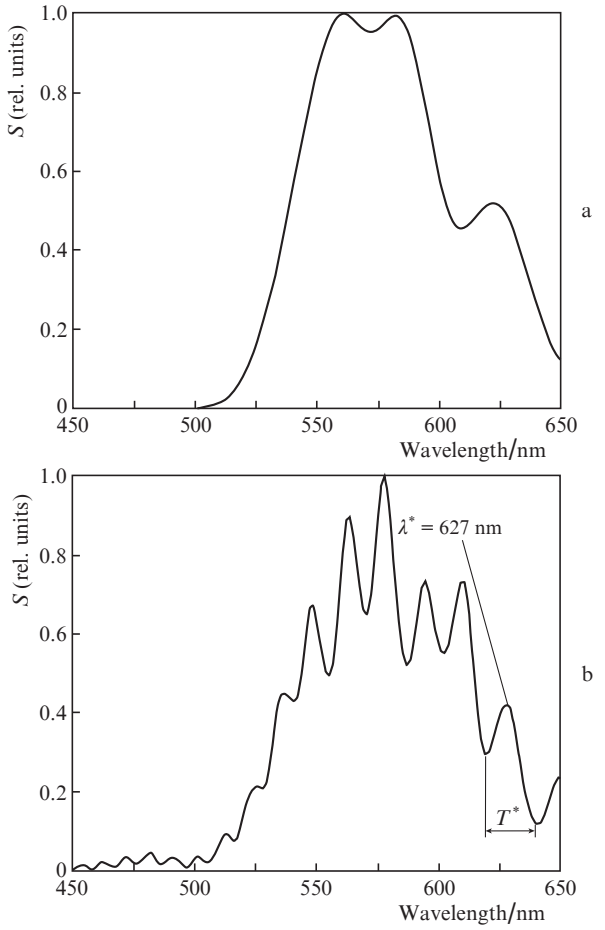

Figure 8. Numerically calculated spectra $S(\lambda)$ in the angular aperture ±0.1 rad for radiation ($W = 50$ μJ) focused by an axicon into a SiO_2 sample in the cases of (a) one LB on $d = 5.5$ mm and (b) two LBs on $d = 6.5$ mm. The distance from the axicon to the sample is $b = 6$ mm.

the LB duration (at an intensity level of e^{-1}) is about 4 fs, the peak intensity reaches 60–100 TW cm^{-2}, and the time intensity profile on the beam axis $I(r = 0,t)$ has a shape characteristic of an LB with a steep trailing edge, caused by defocusing

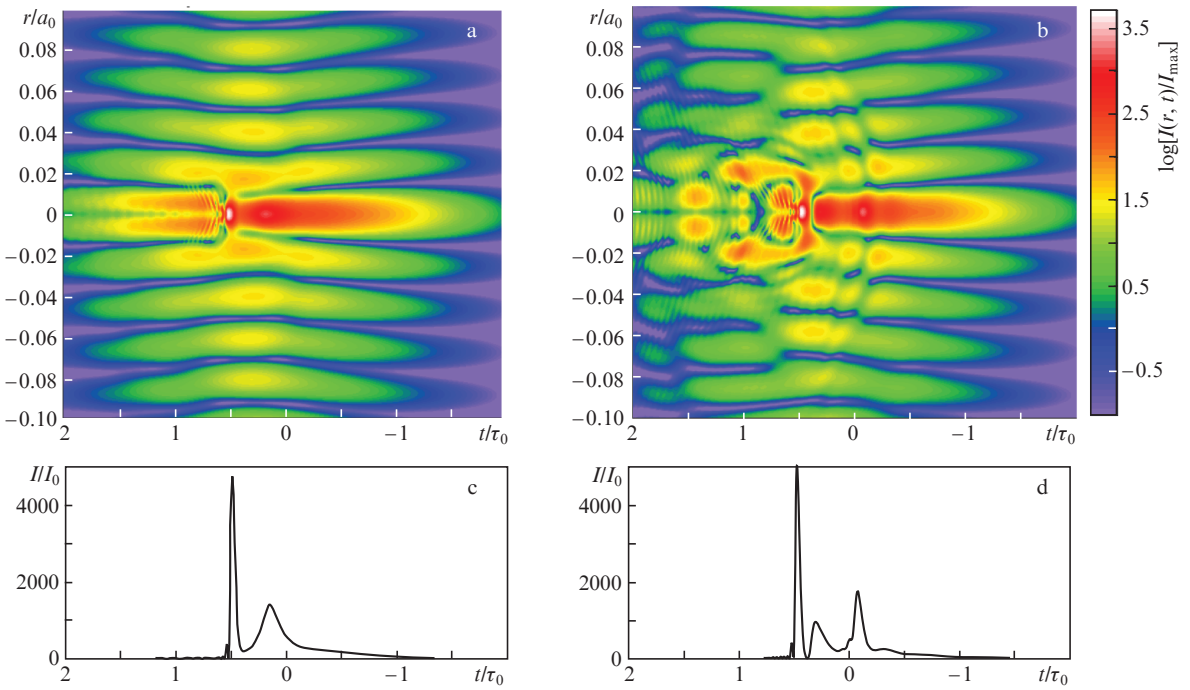

Figure 9. (Colour online) (a, b) Spatio-temporal distributions of intensity $I(r,t)$ in a wave packet and (c, d) time intensity profiles $I(t)$ on the axis when reaching a maximum of intensity (a, c) in the first LB formed at a distance $z = 11$ mm from the axicon tip and (b, d) in the second LB formed at a distance $z = 12.5$ mm. The distance from the axicon to the sample is $b = 6$ mm. The pulse energy is $W = 50$ μJ, the initial intensity is $I_0 = 11.9$ GW cm^{-2}, and the peak intensity in the LB is $I_{max} = 60$ TW cm^{-2}. The radiation propagates from left to right.

radiation on the self-induced laser plasma (Figs 9c and 9d). In the spatio-temporal intensity distribution $I(r,t)$ in the LB, as well as in the case of filamentation under normal group velocity dispersion conditions, the LB-tail defocusing on plasma manifests itself in the form of a narrow low-intensity region that follows the intensity peak (Figs 9a and 9b).

At the same time, the propagation of an LB formed in a Bessel–Gaussian beam is affected by the ring beam structure. The rings in the Bessel–Gaussian profile are drawn up to the beam centre (Figs 9a and 9b). Thus, they increase the energy on the beam axis and play a role of an additional energy reservoir, supporting the energy localisation in the LB. The effect of drawing up rings to the wave packet centre, along with the energy transfer from adjacent temporal layers to the LB-formation region (with a length of $\sim 0.5\tau_0$) under conditions of self-phase modulation, facilitates the formation of the second LB, which has the same parameters as the first one in this case (Figs 9b and 9d).

Oscillations of the spectral components' intensity $S(\lambda)$ for the anti-Stokes wing of the supercontinuum in an angular aperture of ±0.1 rad were obtained numerically for an LB sequence in fused silica and calcium fluoride at different distances b between the axicon tip and samples. On a logarithmic scale, the relative change in the oscillation period T/T^* in the spectrum is a linear function of the relative spectral-component wavelength λ/λ^* for the LBs that are formed both in SiO_2 and CaF_2 (Fig. 10). The thus obtained dependences are close to the experimental ones (see Fig. 5).

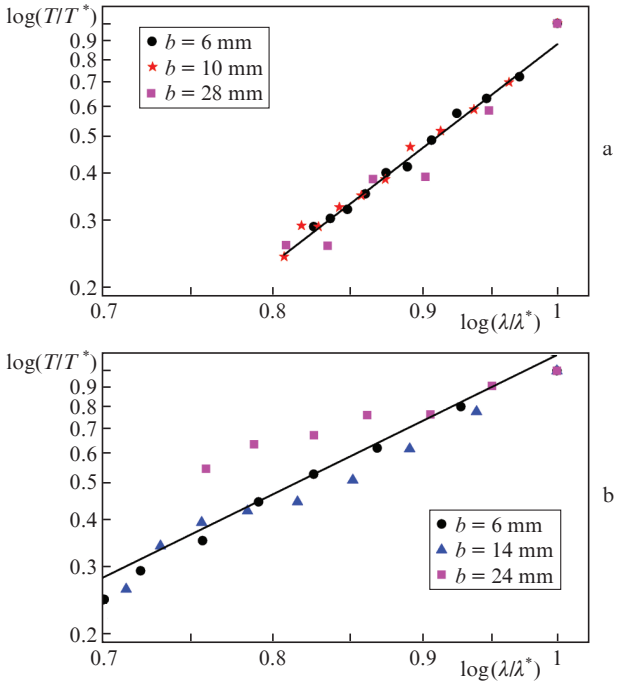

Figure 10. Relative change in the oscillation period T/T^* of spectral components as a function of their wavelength λ/λ^* on a logarithmic scale, according to the results of numerical calculations at different distances b between the axicon and the input face of (a) fused silica (a) and (b) calcium fluoride samples. The solid line is an approximation.

4. Interference analysis

The analysis is based on the model according to which an LB is a moving point source, emitting a broadband supercontinuum on its path length l. The supercontinuum components emitted by an LB at different points on the path length are phase-shifted due to the difference between the phase velocity $c_0/n(\lambda)$ of the spectral component at the wavelength λ and the

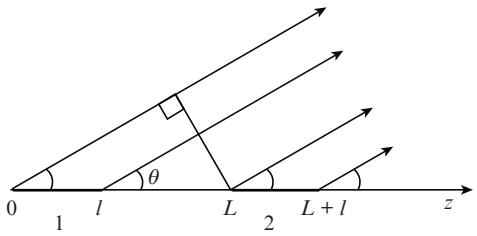

Figure 11. Interference model of the formation of a frequency-angular supercontinuum spectrum in the case of generation of two LBs. The LB emission regions are denoted as 1 and 2.

pulse group velocity v_g at the wavelength λ_0. In the case of two LBs spaced by a distance L, a phase shift arises for the spectral components emitted by both LBs (Fig. 11).

Let us assume for simplicity that the amplitude $A(\lambda,\theta,z)$ of a supercontinuum spectral component is independent of the wavelength λ of a wave that propagates at an angle θ with respect to the LB propagation direction and does not change on the LB path length. Then the amplitude at a point z on the LB path length has the form

$$A(\lambda,\theta,z) = A_0\exp[i\varphi(\lambda,\theta,z)]. \quad (3)$$

The phase shift of the LB-emitted spectral components is

$$\varphi(\lambda,\theta,z) = k_0\left[\left(1-\frac{\lambda_0}{\lambda}\right)\frac{c_0}{v_g} - \left(1-\frac{\lambda_0 n(\lambda)}{\lambda n_0}\right)\cos\theta\right]z,\ k_0 = \frac{2\pi}{\lambda_0}. \quad (4)$$

In correspondence with Fig. 11 and expression (3), the spectral-component amplitude $A(\lambda,\theta)$ (being the result of interference of both LB radiations) takes the form

$$A(\lambda,\theta) = A_0\int_0^l \exp[i\varphi(\lambda,\theta,z)]\,dz\,\{1+\exp[i\varphi(\lambda,\theta,L)]\}. \quad (5)$$

Hence, the frequency-angular emission spectrum of the supercontinuum of two LBs can be written as

$$S(\lambda,\theta) = 4A_0^2 l^2\,\mathrm{sinc}^2\left[\frac{\varphi(\lambda,\theta,l)}{2}\right]\cos^2\left[\frac{\varphi(\lambda,\theta,L)}{2}\right]. \quad (6)$$

The first factor in expression (6) determines the formation of an isolated anti-Stokes wing in the spectrum of an LB with a path length l. The second factor, related to the occurrence of another LB at a distance L from the first one, describes the spectrum modulation as a function of the spectral-component wavelength λ and angle θ. The oscillation period of the spectral components' intensity is independent of the pulse duration, energy and radius, as well as the focusing conditions, but is determined by the material dispersion of the medium, $n(\lambda)$, and the distance L between the light bullets formed under conditions of anomalous group velocity dispersion.

The spectrum $S_{\theta_0}(\lambda)$ in the angular aperture $2\theta_0$, which is due to the superposition of the spectral components propagating at an angle $\theta \leqslant \theta_0$, is determined by the expression

$$S_{\theta_0}(\lambda) = \left[\int_{-\theta_0}^{+\theta_0} A(\lambda,\theta)\,d\theta\right]^2. \quad (7)$$

Figure 12 shows the spectra $S_{\theta_0}(\lambda)$ of the anti-Stokes wing on the filament axis in fused silica, calculated from formulae (4)–(7) for one LB and for two LBs spaced at different distances L: 1.5 and 2.5 mm. It can be seen that, as well as in the experiment, the anti-Stokes wing spectral intensity gradually changes with wavelength (Fig. 12, dashed line), whereas the formation of the second LB leads to the occurrence of oscillations in the spectrum (Fig. 12, solid lines). One can see that an increase in the distance between LBs from 1.5 to 2.5 mm reduces the oscillation period in the spectrum, which is determined as the interval between the wavelengths of adjacent minima of spectral components' intensity.

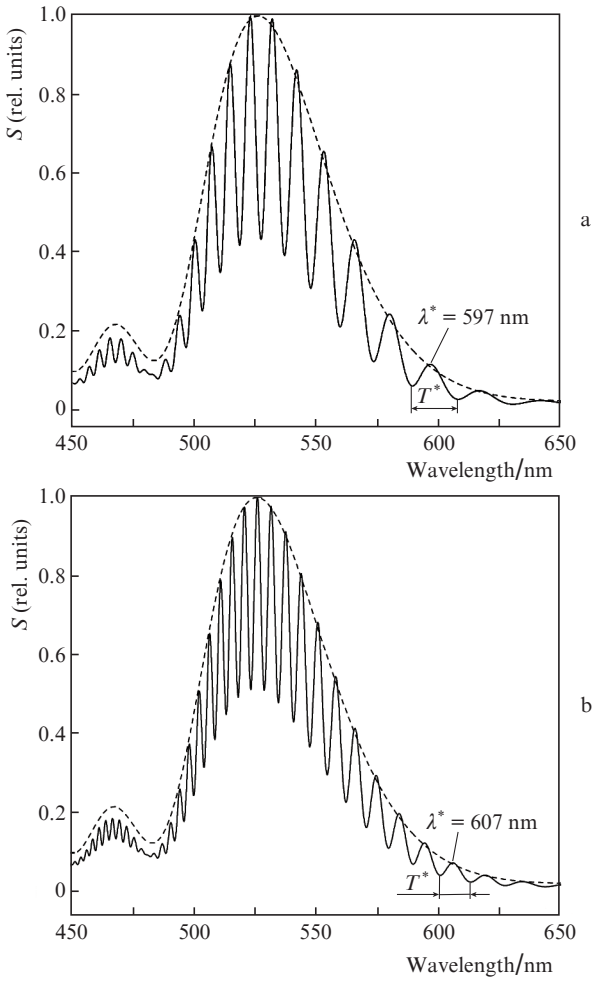

Figure 12. Spectra of the anti-Stokes wing of a supercontinuum during the LB formation at a wavelength of 1900 nm in fused silica, calculated within the interference model: (dashed line) one LB and (solid line) two LBs spaced by a distance L = (a) 1.5 or (b) 2.5 mm.

The dependence of the relative oscillation period of the intensity of spectral components on their wavelength, calculated within the interference model, is presented in Fig. 13 on a logarithmic scale. The dependence of $\log(T/T^*)$ on $\log(\lambda/\lambda^*)$ is linear at different distances L between the LBs, which is consistent with both experimental (Fig. 5) and numerical results (Fig. 10).

The data obtained on the basis of the interference analysis confirm the decisive role of the formation of the second LB as another source of a supercontinuum in the occurrence of modulation in the anti-Stokes band spectrum. The interference model explains also the modulation (recorded in [8]) in

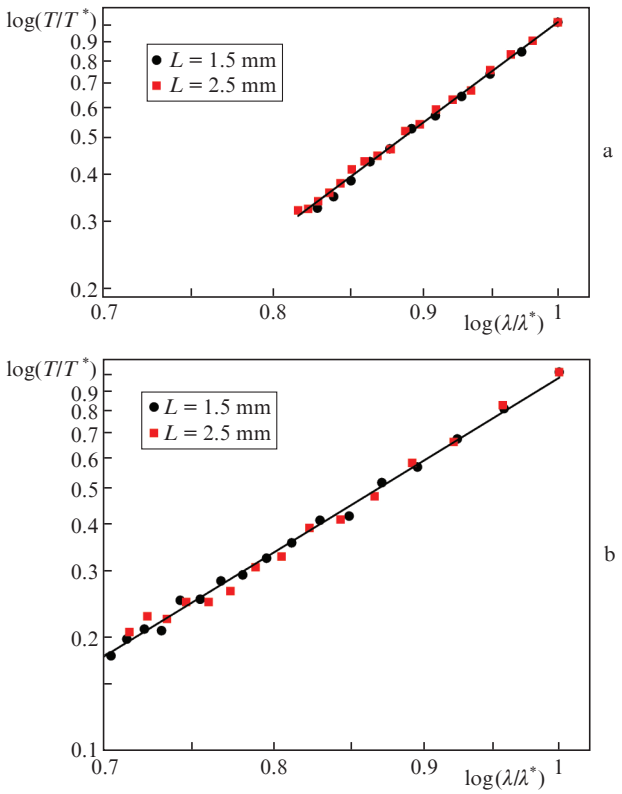

Figure 13. Relative change in the oscillation period T/T^* of spectral components with a change in their wavelength λ/λ^* on a logarithmic scale (obtained within the interference model) at different distances L between LBs for (a) fused silica and (b) calcium fluoride samples. The solid line is an approximation.

the spectrum of 800-nm radiation when the second source of supercontinuum arises due to the refocusing under filamentation in a YAG crystal.

The linearity of the logarithmic dependence of the relative oscillation period T/T^* of spectral components on their wavelength λ/λ^* follows from a simple analysis of the phase shift of these components, emitted by two LBs. Depending on the component frequency ω, the phase shift at $\theta = 0$ is determined as

$$\varphi(\omega, \theta = 0, L) = \left\{\frac{\omega_0 - \omega}{v_g} - [k_0 - k(\omega)]\right\} L. \qquad (8)$$

Using the second-order approximation of the dispersion theory for wave number $k(\omega)$ at point $k(\omega_{as})$ (ω_{as} is the frequency of a spectral maximum of an anti-Stokes wing intensity), one can easily derive an expression for the oscillation frequency of spectral components, $\Omega = \partial\varphi(\omega, \theta = 0, L)/\partial\omega$, as a function of their frequency ω:

$$\Omega = L\left[\frac{1}{v_g(\omega_{as})} - \frac{1}{v_g} + \frac{\partial^2 k}{\partial\omega^2}(\omega - \omega_{as})\right]. \qquad (9)$$

The oscillation frequency Ω of the intensity of spectral components is proportional to their frequency ω, which corresponds to the linear dependence of the relative oscillation period $\log(T/T^*)$ on the wavelength $\log(\lambda/\lambda^*)$ on a logarithmic scale. Note that the consideration of next orders in the expansion of $k(\omega)$ leads to deviations of no more than 10% in the linear dependence (9), obtained in the second-order dispersion approximation.

5. Conclusions

A stable LB sequence is formed in the case of filamentation under conditions of anomalous group velocity dispersion of a femtosecond Gaussian beam focused by an axicon. The occurrence of another supercontinuum source as a result of the formation of the next LB due to the wave packet compression in time under anomalous group velocity dispersion conditions leads to oscillations of spectral component intensity in the anti-Stokes wing; the reason is the interference of the broadband coherent LB-emitted supercontinuum.

The oscillation period, which is defined as the interval between the wavelengths of adjacent minima of spectral component intensity, depends on the distance between the LBs and decreases with an increase in this distance. As follows from the results of spectroscopic measurements, numerical simulation, and analytical study within the interference model, the relative change in the oscillation period of the spectral component intensity for the anti-Stokes wing of LB spectrum in fused silica and calcium fluoride is proportional to the component wavelength on a logarithmic scale and independent of the pulse energy and position of the LB formation region in the filament. According to the interference analysis, the change in the relative oscillation period of the intensity of spectral components in the anti-Stokes wing of the LB spectrum as a function of their wavelength is determined by the dispersion of the medium.

Acknowledgements. The theoretical study was supported by a grant of the Russian Science Foundation (Project No. 18-12-00422), and the experiments were performed within the Extreme Light Fields and Their Interaction with Matter Programme of the Presidium of the Russian Academy of Sciences.

References

1. Pyatnitsky L.N. *Volnovye besselevy puchki* (Wave Besselian Beams) (Moscow: Fizmatlit, 2012) pp 9, 231.
2. Kosareva O.G., Grigor'evskii A.V., Kandidov V.P. *Quantum Electron.*, **35**, 1013 (2005) [*Kvantovaya Elektron.*, **35**, 1013 (2005)].
3. Akturk S., Zhou B., Franco M., Couairon A., Mysyrowicz A. *Opt. Commun.*, **282**, 129 (2009).
4. Abdollahpour D., Panagiotopoulos P., Turconi M., Jedrkiewicz O., Faccio D., Di Trapani P., Couairon A., Papazoglou D.G., Tzortzakis S. *Opt. Express*, **17**, 5052 (2009).
5. Chekalin S.V., Dokukina A.E., Smetanina E.O., Kompanets V.O., Kandidov V.P. *Quantum Electron.*, **44**, 570 (2014) [*Kvantovaya Elektron.*, **44**, 570 (2014)].
6. Nagura C., Suda A., Kawano H., Obara M., Midorikawa K. *Appl. Opt.*, **41**, 3735 (2002).
7. Kandidov V.P., Kosareva O.G., Golubtsov I.S., Liu W., Becker A., Akozbek N., et al. *Appl. Phys. B: Lasers and Optics*, **77**, 149 (2003).
8. Dubietis A., Tamošauskas G., Šuminas R., Jukna V., Couairon A. *Lithuanian J. Physics*, **57**, 113 (2017).
9. Dubietis A., Polesana P., Valiulis G., Stabinis A., Di Trapani P., Piskarskas A. *Opt. Express*, **15**, 4168 (2007).
10. Chekalin S.V., Kompanets V.O., Dormidonov A.E., Kandidov V.P. *Usp. Fiz. Nauk*, **189**, 299 (2019).
11. Chekalin S.V., Kompanets V.O., Zaloznaya E.D., Kandidov V.P. *Quantum Electron.*, **49**, 344 (2019) [*Kvantovaya Elektron.*, **49**, 344 (2019)].

12. Smetanina E.O., Kompanets V.O., Chekalin S.V., Kandidov V.P. *Quantum Electron*., **42**, 913 (2012) [*Kvantovaya Elektron*., **42**, 913 (2012)].
13. Smetanina E.O., Kompanets V.O., Chekalin S.V., Kandidov V.P. *Quantum Electron*., **42**, 920 (2012) [*Kvantovaya Elektron*., **42**, 920 (2012)].
14. Smetanina E.O., Kompanets V.O., Chekalin S.V., Dormidonov A.E., Kandidov V.P. *Opt. Lett*., **38**, 16 (2013).
15. Durand M., Lim K., Jukna V., McKee E., Baudelet M., Houard A., Richardson M., Mysyrowicz A., Couairon A. *Phys. Rev. A*, **87**, 043820 (2013).
16. Dormidonov A.E., Kompanets V.O., Chekalin S.V., Kandidov V.P. *Opt. Express*, **23**, 29202 (2015).
17. Chekalin S.V., Dormidonov A.E., Kompanets V.O., Zaloznaya E.D., Kandidov V.P. *J. Opt. Soc. Am. B*, **36**, A43 (2019).
18. Dormidonov A.E., Kompanets V.O., Kandidov V.P., Chekalin S.V. *Quantum Electron*., **39**, 653 (2009) [*Kvantovaya Elektron*., **39**, 653 (2009)].
19. Kompanets V.O., Chekalin S.V., Kosareva O.G., Grigor'evskii A.V., Kandidov V.P. *Quantum Electron*., **36**, 821 (2006) [*Kvantovaya Elektron*., **36**, 821 (2006)].
20. Dormidonov A.E., Kandidov V.P. *Laser Phys*., **19**, 1993 (2009).
21. Dormidonov A.E., Kandidov V.P., Kompanets V.O., Chekalin S.V. *JETP Lett*., **91**, 373 (2010) [*Pis'ma Zh. Eksp. Teor. Fiz*., **91**, 405 (2010)].
22. Kandidov V.P., Smetanina E.O., Dormidonov A.E., Kompanets V.O., Chekalin S.V. *Zh. Eksp. Teor. Fiz*., **140**, 484 (2011).
23. Dormidonov A.E., Kompanets V.O., Chekalin S.V., Kandidov V.P. *Pis'ma Zh. Eksp. Teor. Fiz*., **104**, 173 (2016).
24. Brabec T., Krausz F. *Phys. Rev. Lett*., **78**, 3282 (1997).
25. Zaloznaya E.D., Kompanets V.O., Dormidonov A.E., Chekalin S.V., Kandidov V.P. *Quantum Electron*., **48**, 366 (2018) [*Kvantovaya Elektron*., **48**, 366 (2018)].